Journal of Palaeogeography, 2026, 15(2): 100338

Available online at www.sciencedirect.com

ScienceDirect

journal homepage: http://www.journals.elsevier.com/journal-of-palaeogeography/

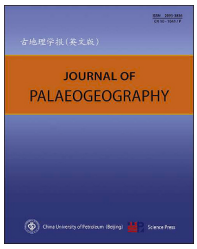

Research article

Cambrian—Ordovician sedimentary environmental evolution and dolomitization in the Lower Yangtze region of China by sedimentary microfacies and geochemistry

Jia-Wei He [a], *Tao Deng* [b], *Li-Juan Wang* [c,d], *Jun-Peng Guan* [c,d], *Yong-Biao Yang* [c,d], *Xiu-Mian Hu* [b,*]

[a] *Institute of Sedimentary Geology, Chengdu University of Technology, Chengdu 610059, Sichuan Province, China*
[b] *School of Earth Sciences and Engineering, Nanjing University, Nanjing 210093, Jiangsu Province, China*
[c] *Geological Survey of Jiangsu Province, Nanjing 210018, Jiangsu Province, China*
[d] *Natural Resources Carbon Neutralization Engineering Research Center of Jiangsu Province, Nanjing 210018, Jiangsu Province, China*

Abstract The Lower Yangtze region in China hosts extensive Early Paleozoic dolomitic sequences, yet their sedimentary environments and genetic mechanisms remain poorly constrained. This study integrates carbonate microfacies analysis with geochemical data (major, trace, and rare earth elements) from three studied sections (Mufushan, Lunshan, Tangshan) and two drill cores (Sure 1 and Sure 2) to elucidate the depositional evolution and dolomitization of the Cambrian—Ordovician Guanyintai, Lunshan, and Honghuayuan formations. Totally 15 types of carbonate microfacies were identified, revealing a transition from supratidal sabkha (e.g., powder-crystal dolostone with geopetal structures) to shallow shoal environments (e.g., dolomitized oolitic grainstone). Geochemical signatures (MgO—CaO covariation, Sr depletion, and REY patterns) indicate that the Guanyintai Formation dolostone formed via reflux penetration of Mg^{2+} enriched brines in shallow burial settings, while the Lunshan Formation experienced superimposed burial and hydrothermal dolomitization, evidenced by saddle dolomite textures and positive δEu anomalies. Contrarily, the Honghuayuan Formation limestones exhibit significant terrigenous input (elevated Al_2O_3, Zr, and SiO_2). This study establishes a dual-phase genetic model for Cambrian—Ordovician dolostone in Lower Yangtze region, emphasizing the interplay of evaporative reflux and hydrothermal activity. These findings provide critical insights for predicting dolostone reservoir distribution and optimizing hydrocarbon exploration in analogous marine carbonate systems.

Keywords Lower Yangtze region, Dolomitization, Carbonate microfacies, Geochemistry, Paleozoic

* Corresponding author.
E-mail address: huxm@nju.edu.cn (X.-M. Hu).
Peer review under responsibility of China University of Petroleum (Beijing)
https://doi.org/10.1016/j.jop.2026.100338

Received 29 December 2024; revised 26 June 2025; accepted 27 January 2026; available online 2 February 2026

1. Introduction

Dolostone, as a critical component of carbonate platforms throughout Earth's history, has long been a focal scientific issue in sedimentology due to its genetic mechanisms and paleoenvironmental implications (Cai *et al.*, 2021; Zhang *et al.*, 2024; Bai *et al.*, 2025). The prevailing academic consensus identifies multiple dolomitization processes, including microbial (biological), sabkha, reflux seepage, burial, hydrothermal, and mixing-zone processes (Van Lith *et al.*, 2003; Metcalfe, 2011; Gregg *et al.*, 2015; Petrash *et al.*, 2017; Cai *et al.*, 2021; Li *et al.*, 2022; Zhang *et al.*, 2024; Zhou *et al.*, 2024). However, the complexity and prolonged nature of dolomitization processes often result in multiple superimposed dolomitization stages within the same stratigraphic unit (He *et al.*, 2020; Li *et al.*, 2022). The Early Paleozoic, marked by global tectonics, including the collision of Yangtze—Cathaysian blocks and Caledonian Orogeny (Zhang *et al.*, 2013; Li *et al.*, 2014; Shu *et al.*, 2021; Shan *et al.*, 2022), provides a unique window to investigate the coevolution of dolomitization processes and paleogeographic configurations. The well-preserved Cambrian—Ordovician carbonate sequences in the Lower Yangtze region of South China, particularly the thick dolostone successions of the Guanyintai and Lunshan formations (Li *et al.*, 2016; Xu *et al.*, 2017; Wu *et al.*, 2020; Guo *et al.*, 2023), serve as an ideal natural laboratory for unraveling multiphase dolomitization dynamics. However, existing studies predominantly focus on the Upper Yangtze region (e.g., Dengying and Longwangmiao formations in the Sichuan Basin) (Jiang *et al.*, 2023; Qu *et al.*, 2023; Shang *et al.*, 2023; Yang *et al.*, 2023; Liu *et al.*, 2024), with limited systematic understanding of the depositional environment evolution, fluid sources, and its coupling with regional tectonic activities in the Lower Yangtze region. These constraints limit the understanding of Early Paleozoic paleoenvironmental reconstruction and dolostone formation mechanisms in the Lower Yangtze Block.

The Lower Yangtze region, located on the northeastern margin of the Yangtze Block, has been in a stable marginal marine environment from the Late Sinian (Ediacaran) to the Early Triassic, accumulating thick carbonate successions dominated by dolostone (Zhang *et al.*, 2006; Li *et al.*, 2016; Xia *et al.*, 2018; Fang *et al.*, 2020; Wu *et al.*, 2020; Guo *et al.*, 2023; Chen *et al.*, 2024). The Caledonian Orogeny further shaped its platform and basin depositional architecture (Zhang *et al.*, 2013; Li *et al.*, 2016; Xia *et al.*, 2018; Chen *et al.*, 2024). Although previous studies proposed that Lower Yangtze dolostone formed through penecontemporaneous multiphase dolomitization with localized hydrothermal influences (Fan *et al.*, 1996; Li *et al.*, 2016; Xu *et al.*, 2017; Guo *et al.*, 2023; Chen *et al.*, 2024), these interpretations rely primarily on petrological or single-proxy geochemical analyses, lacking integrated constraints from carbonate microfacies and multi-proxy geochemical datasets. Additionally, extensive surface coverage in the region limits outcrop-based investigations, resulting in incomplete characterization of fluid sources and spatiotemporal linkages between dolomitizing fluids and tectonic—eustatic events. These limitations have hindered a holistic understanding of dolostone genesis in this tectonically active margin.

This study focuses on three measured sections in the Nanjing Ningzhen area, and two wells (Sure 1 and Sure 2) in the Yancheng City, employing an integrated approach combining carbonate microfacies analysis with geochemical proxies (major and trace elements, and rare earth elements including yttrium), to investigate the formation environment and genetic mechanisms of dolostone in the Lower Yangtze region. The study aims to establish a dolostone genetic model for the Lower Yangtze region, providing a regional comparative case for Early Paleozoic carbonate platform dolostone research globally.

2. Geological background

The Lower Yangtze region, situated in the northeastern Yangtze Block, covers an area of 22.5×10^4 km^2 across Jiangsu, Zhejiang, Anhui, Jiangxi Provinces, and Shanghai City (Cai *et al.*, 2015; Shu *et al.*, 2021). It is bounded by the Tancheng-Lujiang Fault to the west, the Sulu Orogen to the northwest, the Jiangshan-Shaoxing Fault to the south, and the Cathaysian Block to the southeast (Wang *et al.*, 2013;

Li *et al.*, 2014). The region connects with the Middle Yangtze region at Jiujiang, Jiangxi Province, to the southwest (Fig. 1A). The tectonic and sedimentary evolution of the Lower Yangtze region comprises two principal stages. During the Jinning-Caledonian phase, northeast-trending synsedimentary faults controlled the development of distinct basin and platform facies, dividing the area into four regions: Area I (Chuzhou-Yancheng basin facies), Area II (Nanjing-Anqing platform facies), Area III (Wuxi-Huangshan basin facies), and Area IV (Yuhang platform facies) (Gao *et al.*, 2023; Guo *et al.*, 2023) (Fig. 1A). This period was characterized by the deposition of extensive marine carbonate sequences (Fig. 1B). The terminal Caledonian collision between the Cathaysian Block and Yangtze Block triggered rapid uplift of the Lower Yangtze region, followed by extensive clastic deposition during the early Silurian (Zhang *et al.*, 2013; Li *et al.*, 2014; Shu *et al.*, 2021). The subsequent Indosinian-Yanshanian phase was dominated by compressional tectonics resulting from the convergence between the Yangtze and North China plates. This phase exhibited contrasting deformation patterns, with intense thrust-nappe structures developing in the northern and southern margins, while the central region maintained relative tectonic stability. During the late Yanshanian period, tectonic quiescence led to regional subsidence and the formation of a residual basin, subsequently modified by marine transgression and foreland basin development (Zhang *et al.*, 2013; Xia *et al.*, 2018; Shu *et al.*, 2021)

2.1. Ningzhen area

The Ningzhen area, situated in Nanjing City, represents a key geological domain within the Nanjing-Anqing Platform from the Late Sinian to Silurian (Fig. 1A). This area is distinguished by extensive Paleozoic marine carbonate sequences (Chai, 2019; Gao *et al.*, 2023; Guo *et al.*, 2023). The Upper Cambrian Guanyintai Formation comprises basal thin- to medium-bedded gray algal dolostone, grading

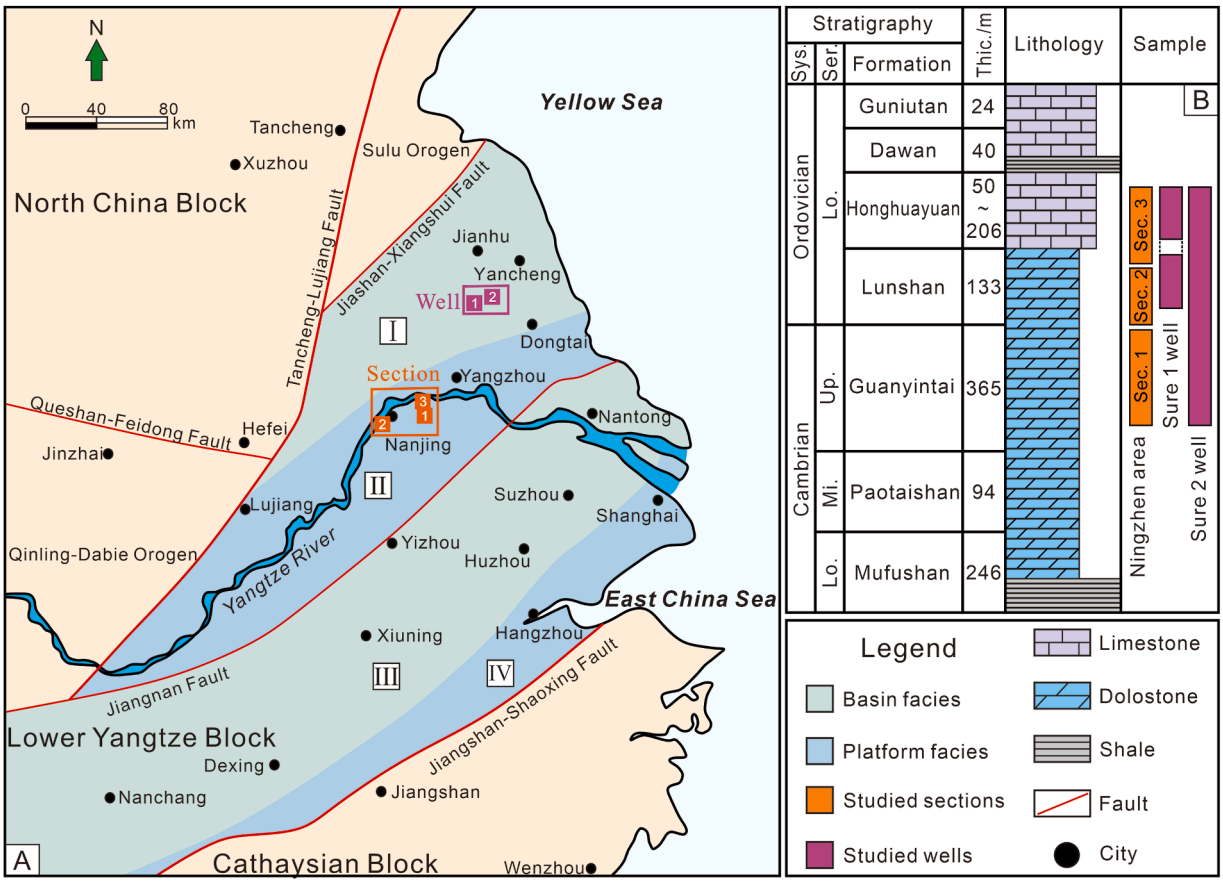

Fig. 1 **A**) Simplified paleogeographical map showing the Cambrian—Ordovician sedimentary areas in the Lower Yangtze region, and locations of the studied sections and wells (modified from Guo *et al.*, 2023). Studied sections (orange box): 1: Mufushan, 2: Lunshan, 3: Tangshan; Studied wells (purple box): 1: Sure 1, 2: Sure 2. The Lower Yangtze Block are divided into four areas: Area I: Chuzhou-Yancheng Basin, Area II: Nanjing-Anqing Platform, Area III: Wuxi-Huangshan Basin, Area IV: Yuhang Platform. **B**) Comprehensive stratigraphic histogram of the Lower Yangtze region showing the sampling positions (modified from Guo *et al.*, 2023).

upward into thick-bedded gray to dark-gray brecciated dolostone. The overlying Lower Ordovician Lunshan Formation initiates with brownish red thin- to medium-bedded dolostone (Fig. 2A, B), containing 0.5—1.0 m diameter siliceous nodules (Fig. 2C), multiple diabase dyke intrusions (Fig. 2D, E), and soft-sediment deformation structures (Fig. 2F). Its upper succession is characterized by dark-gray to grayish-black medium- to coarse-grained dolostone (Fig. 2G), locally interbedded with gray medium- to thick-bedded limy dolostone and dolomitic limestones containing chert bands. The overlying Lower Ordovician Honghuayuan Formation consists of basal light gray- to dark-gray thick-bedded peloidal sparitic limestone with calcite-filled paleokarst cavities (Fig. 2H), capped by gray bioclastic and oolitic limestones (Fig. 2I).

2.2. *Sure 1 and 2 wells*

The Sure 1 and 2 wells are located in the Yancheng City, situated in the Chuzhou-Yancheng Basin (Chai,

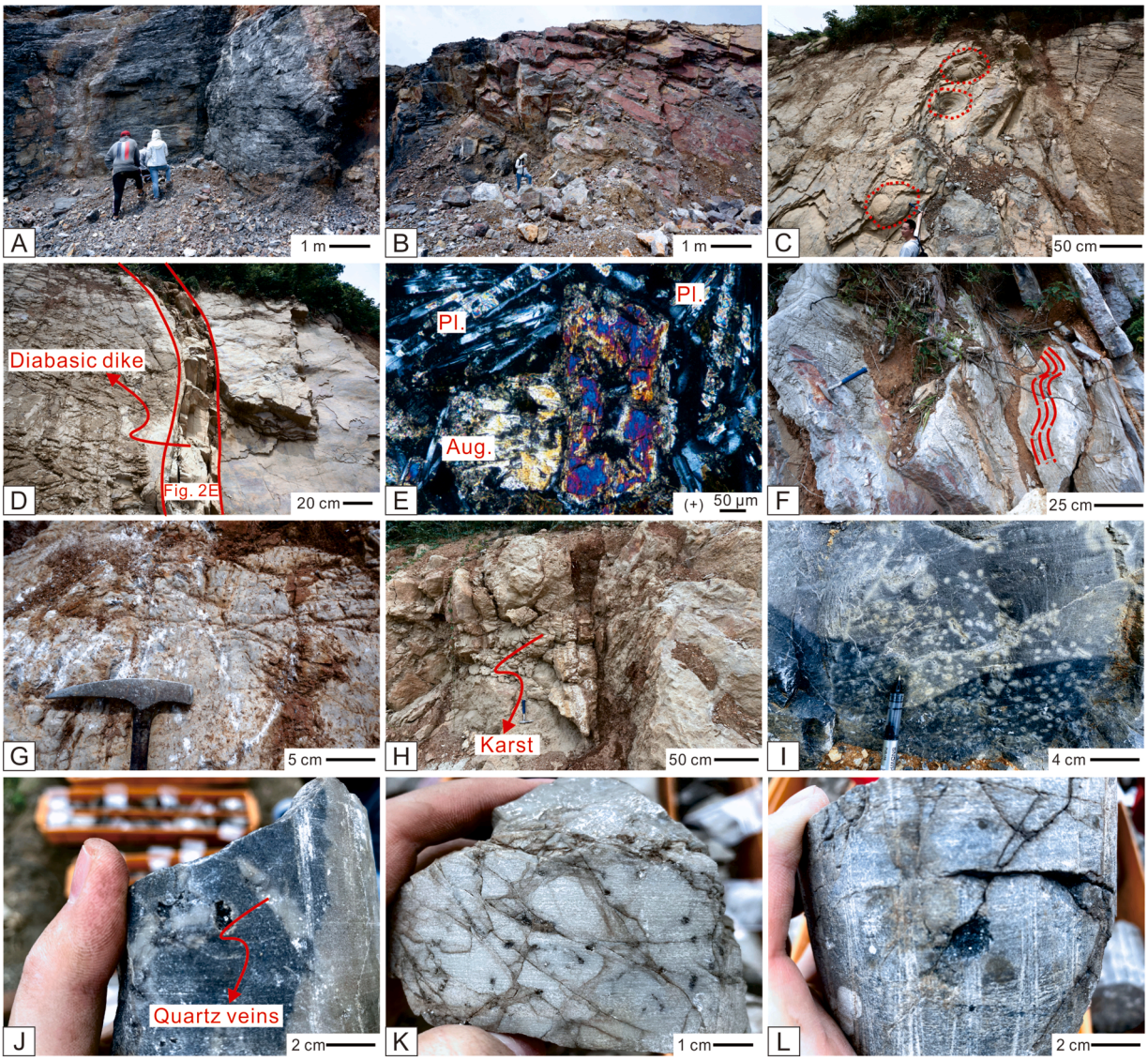

Fig. 2 Outcrop photographs of the Lunshan (**A**—**G**) and Honghuayuan (**H, I**) formations in Ningzhen area, and core photographs of Sure 1 (**J**) and Sure 2 (**K, L**) wells. **A**) Thin-bedded dolostone; **B**) Thin- to medium-bedded dolostone (person for scale is ~1.65 m high); **C**) Siliceous nodules (circles); **D**) Diabase dykes (red lines); **E**) Microstructure of diabase dikes under cross-polarized light (+). Pl.: Plagioclase, Aug.: Augite; **F**) Cleaved and soft-sediment deformation (red dotted lines); **G**) Dark-gray to grayish-black medium- to coarse-grained dolostone; **H**) Karst caves; **I**) Dark gray dolomitic peloidal packstone; **J**) Gray-black powder-crystal dolostone in the Lunshan Formation of the Sure 1 well; **K**) Gray brecciated dolostone in the Guanyintai Formation of the Sure 2 well; **L**) Gray-white dolomitized bioclastic packstone in the Honghuayuan Formation of the Sure 2 well.

2019) (Fig. 1A). These wells have penetrated a complete stratigraphic succession from the Cambrian Guanyintai Formation to the Ordovician Lunshan and Honghuayuan formations. In the Sure 1 well, the Lunshan Formation is characterized by grayish-black, fine-crystalline dolostone extensively crosscut by quartz veins (Fig. 2J). The overlying Honghuayuan Formation primarily comprises light gray to white bioclastic limestone and calcarenite, with occasional oolitic limestone interbeds. The Sure 2 well exhibits similar lithological characteristics with variations in rock textures. The Guanyintai Formation is mainly represented by grayish-white, fine-crystalline dolostone with gray, medium-crystalline dolostone, displaying characteristic brecciated textures (Fig. 2K). The Lunshan Formation is composed of gray, fine-crystalline dolostone interbedded with gray residual doloarenite. The Honghuayuan Formation consists predominantly of grayish-white and dolomitized bioclastic packstone and bioclastic limestones (Fig. 2L).

3. Samples and methods

3.1. Samples

Samples were collected from three sections (Mufushan, Lunshan, and Tangshan) and two wells (Sure 1 and Sure 2) (Fig. 1). The 70-m-thick Mufushan section is dominated by Guanyintai Formation dolostones, providing 24 samples (NJ94—NJ117) (Fig. 3A). The 250-m-thick Lunshan section primarily exposes dolostone of the Lunshan Formation, with 82 samples collected (NJ01—NJ82) (Fig. 3A). The 25-m-thick Tangshan section spans the Lunshan and Honghuayuan formations (Fig. 3A), yielding 11 samples (NJ83—NJ93). During sampling, unweathered specimens free of calcite veins and significant diagenetic alteration were prioritized to ensure the integrity of paleoenvironmental records. The Sure 1 well includes the Lunshan and Honghuayuan formations (Fig. 3B),

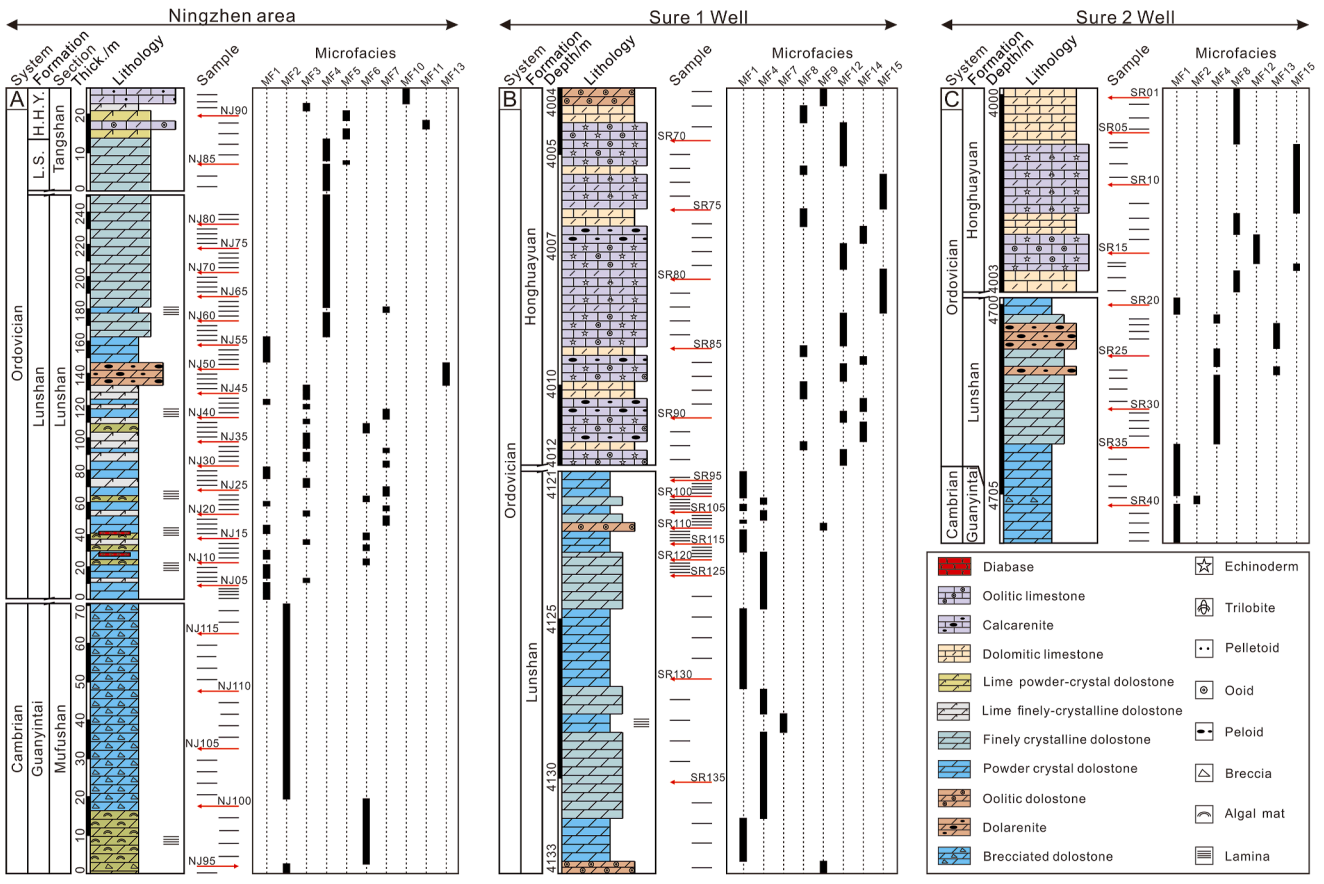

Fig. 3 Stratigraphic log of the Mufushan, Lunshan, Tangshan sections, and the Sure 1 and 2 wells in the Lower Yangtze region, showing sampling locations and microfacies classification. Thick.: Thickness; L.S.: Lunshan; H.H.Y.: Honghuayuan.

with 73 samples collected (SR67—SR139). The Sure 2 well penetrates the Guanyintai, Lunshan, and Honghuayuan formations (Fig. 3C), providing 44 samples (SR01—SR44). All samples avoided intervals affected by drilling-induced fractures or secondary mineralization. A total of 234 samples were analyzed for carbonate microfacies and 44 for geochemical measurements.

3.2. Carbonate microfacies analysis

Microfacies classification integrates field observations with thin section analysis, focusing on grain-size distribution, matrix composition, textural characteristics, biogenic components, mineralogical assemblages, and sedimentary structures (Flügel, 2010). It also considers the dolomitization intensity assessment. For mineral discrimination, rock thin sections are treated with alizarin red S staining, enabling precise differentiation between calcite (stained red) and dolomite (unreacted with characteristic rhombic morphology). Carbonate rocks are categorized using the Dunham's (1962) classification scheme as modified by Embry and Klovan (1971). Dolostone nomenclature follows an integrated classification system combining Folk's (1962) compositional—structural criteria with Randazzo and Zachos' (1984) textural continuum. Environmental interpretation adheres to Wilson's (1975) sedimentary environment classification framework integrated with Flügel's (2010) standard microfacies methodology.

3.3. Geochemical analysis

In the Mineral Separation Laboratory at Nanjing University, 44 fresh core samples from the Sure 2 well were initially crushed and manually purified to remove any potential contaminants, followed by pulverization to a fine powder (<200 mesh) using an agate mill to ensure homogeneity and avoid cross-contamination. These powdered samples were sent to Wuhan SampleSolution Analytical Technology Co. Ltd. Under the conditions of temperature (20—25 °C), relative humidity (10%—30%), voltage (50 kV), and current (60 mA), they were tested for the content of major, trace, and rare earth elements (including yttrium, REY) in the whole rock using X-ray fluorescence (XRF, Primus II, Rigaku, Japan) and Inductively Coupled Plasma Mass Spectrometry (ICP-MS, Agilent 7700e), respectively. Detailed procedures for analytical methods are provided in the supplementary data.

4. Results

4.1. Carbonate microfacies

In the Lower Paleozoic of the Ningzhen area and the Sure 1 and 2 wells, two lithological types have been identified: dolostone (Guanyintai and Lunshan formations) and limestone (Honghuayuan Formation). Through carbonate microfacies analysis, a total of 15 microfacies types were recognized (Figs. 3, 4; Table 1).

4.1.1. MF1: Powder-crystal dolostone

This microfacies occurs in the Guanyintai Formation (Sure 2 well) and Lunshan Formation (Lunshan section and Sure 1 well) (Fig. 3A, B, C). It consists predominantly of equant powder-crystal dolomite (Fig. 4A), exhibiting powder-crystal texture and geopetal structures. The absence of both laminae and biogenic components indicates deposition in a supratidal sabkha environment above mean high-water level (Flügel, 2010).

4.1.2. MF2: Brecciated dolostone

This microfacies occurs in the Guanyintai Formation (Mufushan section and Sure 2 well) (Fig. 3A, C). It comprises bimodal powder-crystal brecciated dolomite, with angular to subangular clasts, poor sorting, and a lack of orientation (Fig. 4B). The absence of both laminae and biogenic components, combined with the textural characteristics, suggests deposition in a supratidal evaporative environment (Flügel, 2010).

4.1.3. MF3: Lime-bearing powder-crystal dolostone

This microfacies occurs in the mid-Lunshan Formation (Lunshan section) and uppermost Honghuayuan Formation (Tangshan section) (Fig. 3A). It consists of >85% equant dolomite (<0.1 mm), exhibiting powder-crystal and bird's eye structures (Fig. 4C). The absence of both laminae and biogenic components, combined with the presence of bird's eye structure, indicates a supratidal sabkha environment above mean high-water level (Wilson, 1975; Flügel, 2010).

4.1.4. MF4: Fine-grained dolostone

This microfacies occurs in the Lunshan Formation (Lunshan and Tangshan sections and Sure 1 and 2

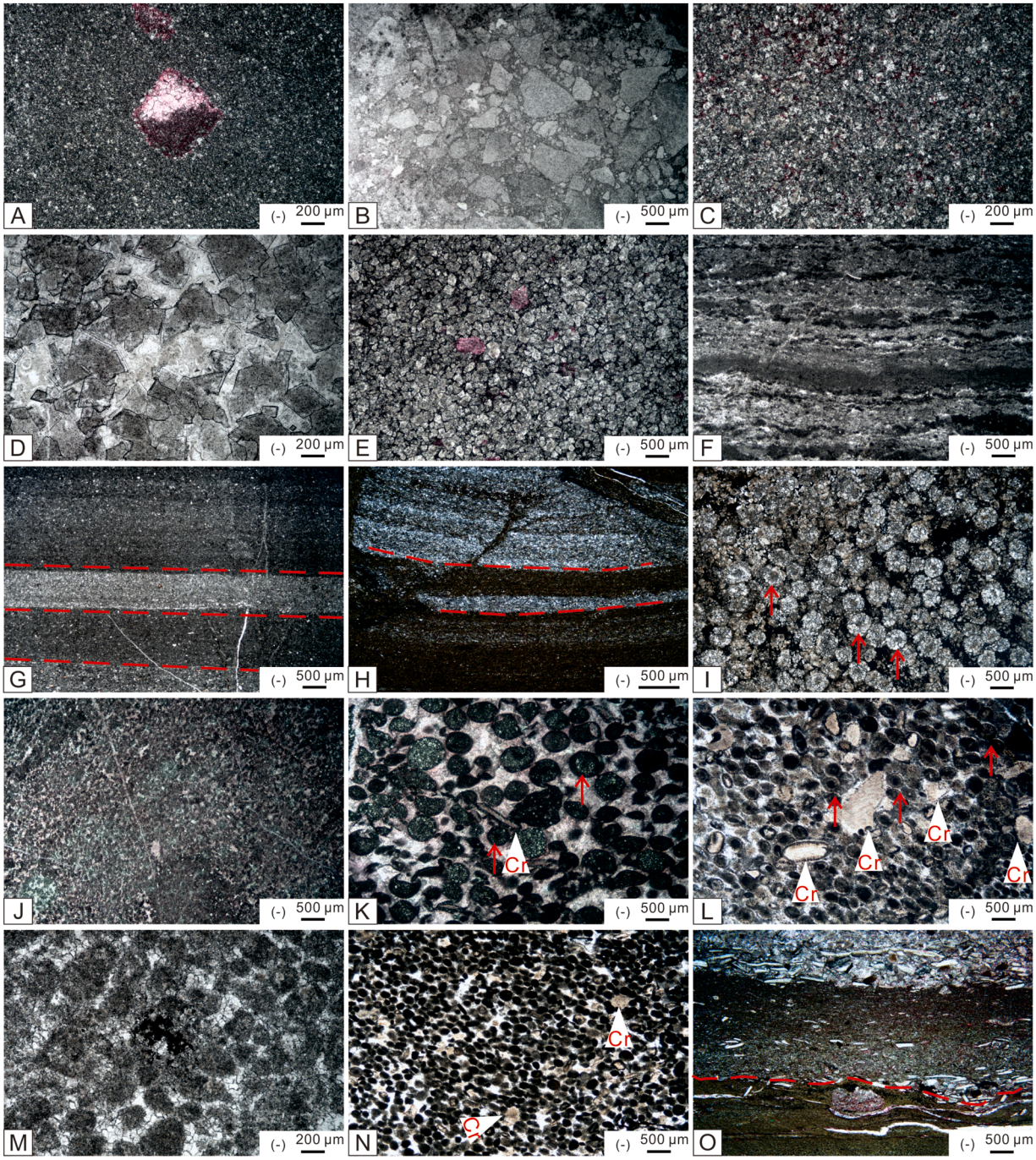

Fig. 4 Microscopic photographs of representative microfacies from Guanyintai, Lunshan, and Honghuayuan formations in the Lower Yangtze region. **A**) MF1 powder-crystal dolostone, showing geopetal structure; **B**) MF2 brecciated dolostone; **C**) MF3 lime-bearing powder-crystal dolostone; **D**) MF4 fine-grained dolostone; **E**) MF5 lime fine-grained dolostone; **F**) MF6 microbial mats, showing irregular laminae and stromatolitic structures; **G**) MF7 laminated powder-crystal dolostone, showing laminated structure (red dotted line); **H**) MF8 dolomitized mudstone; **I**) MF9 residual oolitic dolostone, showing residual oolitic cores (red arrow); **J**) MF10 dolomitic peloidal packstone; **K**) MF11 dolomitized oolitic grainstone, showing residual oolitic (red arrow); **L**) MF12 crinoid oolitic grainstone, showing micrite envelope structure (red arrow); **M**) MF13 residual peloid dolostone; **N**) MF14 peloid grainstone; **O**) MF15 dolomitized bioclastic packstone, showing bioclast layer formed by storm, erosion contact relationship (red dotted line). Cr: crinoid; (-): plane-polarized light.

Table 1 Description and environmental interpretation of the Early Paleozoic Carbonate in the Lower Yangtze area.

Microfacies		Main mineral and particle components	Texture type	Sedimentary structures	Water energy	Depositional environment
MF1	Powder-crystal dolostone	Dolomite	Powder-crystal	Geopetal	Low—medium	Supratidal
MF2	Brecciated dolostone	Dolomite	Powder-crystal, brecciated		Low—medium	Supratidal
MF3	Lime-bearing powder-crystal dolostone	Dolomite, calcite	Powder-crystal	Bird's eye	Low—medium	Supratidal
MF4	Fine-grained dolostone	Dolomite	Fine-grained		Low—medium	Supratidal
MF5	Lime fine-grained dolostone	Calcite, dolomite	Fine-grained, relict grain texture		Low—medium	Upper intertidal
MF6	Microbial mats dolostone	Dolomite, algal mat	Powder-crystal,	Irregular laminae, fenestral	Low	Intertidal
MF7	Laminated powder-crystal dolostone	Dolomite	Powder-crystal	Laminated	High	Intertidal
MF8	Dolomitized mudstone	Calcite, dolomite, bioclast	Micritic	Laminated	High	Intertidal
MF9	Residual oolitic dolostone	Dolomite, ooid	Relict grain texture		Medium	Lagoon
MF10	Dolomitic peloidal packstone	Calcite, peloid	Micritic		Medium—high	Lagoon
MF11	Dolomitized oolitic grainstone	Calcite, ooid, peloid	Relict grain texture	Directional	Medium—high	Lagoon
MF12	Crinoid oolitic grainstone	Calcite, ooid, bioclast	Micritic	Micrite envelope	Medium—high	Lagoon—shallow bank
MF13	Residual peloid dolostone	Dolomite, ooid	Relict grain texture		Medium—high	Lagoon—shallow bank
MF14	Peloid grainstone	Calcite, peloid, bioclast	Relict grain texture	Directional	Medium—high	Shallow shoal
MF15	Dolomitized bioclastic packstone	Calcite, bioclast	Micritic	Laminated	High	Near storm wave base

wells) (Fig. 3A, B, C). It consists of fine-grained dolomite (0.1—0.2 mm), exhibiting subhedral to euhedral crystals and fine-grained structure, displaying foggy cores with bright edges, and saddle dolomite textures (Fig. 4D). The absence of both laminae and biogenic components indicates a supratidal evaporative environment. Notably, crystal size and euhedral morphology increase proximal to quartz veins, suggesting hydrothermal activity influence on dolomitization.

4.1.5. MF5: Lime fine-grained dolostone

This microfacies occurs in the mid-Honghuayuan Formation (Tangshan section) (Fig. 3A). It consists predominantly of equant dolomite (Fig. 4E), exhibiting fine-grained texture. The absence of both laminae and biogenic components, coupled with the lack of evaporitic minerals or exposure structures, suggests deposition in the upper intertidal zone under moderate salinity conditions (Flügel, 2010).

4.1.6. MF6: Microbial mats dolostone

This microfacies occurs in the Guanyintai Formation (Mufushan section) and Lunshan Formation (Lunshan section) (Fig. 3A). It consists of alternating dark-colored laminae (<50 μm) and sparry dolomite crystals (Fig. 4F). The absence of calcified algal cellular structures, combined with the development of fenestral structures, indicates a cyanobacteria-dominated microbial mat origin (Riding, 2000). Locally observed stromatolitic domal structures (Fig. 4F) demonstrate the mat's grain-trapping and binding functions (Noffke and Awramik, 2013). These sedimentary features are a typical indicator of the intertidal zone (Flügel, 2010).

4.1.7. MF7: Laminated powder-crystal dolostone

This microfacies occurs in the Lunshan Formation (Lunshan section and Sure 1 well) (Fig. 3A, B). It consists of >95% bimodal powder-crystal dolomite, exhibiting powder-crystal structure, displaying well-developed laminated structures (Fig. 4G). The absence of both biogenic components and evaporite minerals, coupled with the laminated structure, indicates deposition in a lower intertidal environment (Wilson, 1975; Flügel, 2010).

4.1.8. MF8: Dolomitized mudstone

This microfacies occurs at the upper and lower contacts of the Honghuayuan Formation (Sure 1 and 2

wells) (Fig. 3B, C). It is dominated by calcite (>85%) and dolomite (<15%). This microfacies exhibits high-energy sedimentary structures, including abraded crinoid fragments, laminated structures, and sharp erosional contacts (Fig. 4H). Furthermore, it is stratigraphically positioned between the intertidal residual oolitic dolostone (MF9) and the shoal crinoid oolitic grainstone (MF12). These characteristics collectively indicate formation in a high-energy intertidal environment with strong hydrodynamic conditions (Wilson, 1975; Flügel, 2010).

4.1.9. MF9: Residual oolitic dolostone

This microfacies occurs in the Lunshan and Honghuayuan formations (Sure 1 well) (Fig. 3B). It consists predominantly of ooids (Fig. 4I), displaying spherical to rounded morphology, good sorting, and particle-supported fabric. The ooids are partially to completely dolomitized, preserving grain structures with occasional intact nuclei. The substantial micritic matrix indicates low hydrodynamic energy. Additionally, the presence of well-preserved ooids with intact radial structures and the absence of open-marine fossils (e.g., corals, brachiopods) collectively suggest deposition in a low-energy restricted lagoon environment (Flügel, 2010).

4.1.10. MF10: Dolomitic peloidal packstone

This microfacies occurs in the Honghuayuan Formation (Tangshan section) (Fig. 3A). It consists of peloids, exhibiting micritic matrix and grain-supported structure (Fig. 4J). The poorly sorted, subspherical to oblate peloids, are predominantly composed of micritic limestone clasts. The absence of both laminae and biogenic components, coupled with the peloids, suggests deposition in a restricted lagoonal environment (Flügel, 2010).

4.1.11. MF11: Dolomitized oolitic grainstone

This microfacies occurs in the Honghuayuan Formation (Tangshan section) (Fig. 3A). It consists predominantly of ooids (Fig. 4K), accompanied by peloids and echinoderm fragments in a grain-supported fabric. The ooids, mostly replaced by powder-crystal dolomite forming a residual grain structure, display spherical to subrounded shapes with radial structures and moderate sorting. The presence of radial ooids and peloids indicates deposition in a restricted lagoon environment (Wilson, 1975; Flügel, 2010).

4.1.12. MF12: Crinoid oolitic grainstone

This microfacies occurs in the Honghuayuan Formation (Sure 1 and 2 wells) (Fig. 3B, C). It consists predominantly of crinoids, ooids, and peloids (Fig. 4L). The matrix is composed of sparitic calcite cement, exhibiting granular texture and supported by particles. Crinoids display coaxial cementation, while ooids exhibit elliptical to spherical morphologies, predominantly of radial and micritic types with well-developed micrite envelope structure. The predominance of radial ooids and sparitic cement corresponds to standard microfacies SMF15 (Flügel, 2010), indicating deposition in a lagoon—shallow bank environment.

4.1.13. MF13: Residual peloid dolostone

This microfacies occurs in the Lunshan Formation (Lunshan section and Sure 2 well) (Fig. 3A, C). It consists predominantly of peloids and ooids (Fig. 4M), exhibiting a residual grain structure and grain-supported fabric. The peloids are well-sorted and subrounded to rounded, consisting predominantly of dolomite. The ooids display elliptical to subrounded morphologies with radial fabrics and extensive dolomitization. The grain-supported texture and compositional characteristics indicate deposition in a lagoon—shallow bank environment (Flügel, 2010).

4.1.14. MF14: Peloid grainstone

This microfacies occurs in the Honghuayuan Formation (Sure 1 well) (Fig. 3B). It consists of peloids and rare crinoid fragments (Fig. 4N), exhibiting a micritic texture and grain-supported fabric. The peloids are subrounded to rounded, with good sorting and a preferred orientation of long axes. The grain-supported texture and micritic matrix, combined with the directional fabric of peloids, indicate deposition in a high-energy shallow shoal environment, corresponding to standard microfacies SMF16 (Flügel, 2010).

4.1.15. MF15: Dolomitized bioclastic packstone

This microfacies occurs in the Honghuayuan Formation (Sure 1 and 2 wells) (Fig. 3B, C). It consists of bioclasts, such as crinoids, bivalves, and trilobites, exhibiting characteristics of directionality and gradation (Fig. 4O). The erosional contact between bioclastic layers and micritic background sediments,

coupled with fragmented bioclasts, indicates sedimentary environment near the storm wave base (Flügel, 2010).

4.2. Geochemistry

4.2.1. Major Elements

The Guanyintai Formation in the Sure 2 well is predominantly composed of CaO (avg. 26.33%) and MgO (avg. 24.69%) (Fig. 5A), and the next most abundant components are Al_2O_3 and SiO_2. The elements composition of the Lunshan Formation closely resembles that of the Guanyintai Formation (Fig. 5B). The dominant components are CaO (avg. 27.02%) and MgO (avg. 24.38%). Secondary component includes Al_2O_3, with an average of 1.52%. SiO_2, Fe_2O_3, Na_2O, K_2O, MnO, P_2O_5, and TiO_2 all have contents below 1%. In contrast, the Honghuayuan Formation in the Sure 2 well is predominantly composed of SiO_2 (avg. 31.64%), CaO (avg. 22.83%), and Al_2O_3 (avg. 10.01%) (Fig. 5C). Secondary components include Na_2O, Fe_2O_3, K_2O, and MgO. The contents of MnO, P_2O_5, and TiO_2 are all below 1%.

4.2.2. Trace elements

The Guanyintai Formation of the Sure 2 well is predominantly contains Sr (avg. 49.5 ppm), Zr (avg. 44.7 ppm), and Sc (avg. 30.6 ppm) (Fig. 5D). The averages of V, Ni, Cu, Pb, Mo, Co, Hf, and Cs are all below 10 ppm. Similarly, the Lunshan Formation is primarily composed of Sr (avg. 25.5 ppm), Zr (avg. 40.0 ppm), and Sc (avg. 28.2 ppm) (Fig. 5E). The averages of Ni, Cu, V, Co, Pb, Hf, Mo, and Cs are all below 10 ppm. In contrast, the Honghuayuan Formation primarily composed of Sr and Zr (Fig. 5F), with concentrations ranging from 169 ppm to 670 ppm (avg. 328 ppm) and 40 ppm to 164 ppm (avg. 102 ppm), respectively. The next most abundant elements are V, Sc, Ni, and Cu.

4.2.3. Rare earth elements and yttrium

The Guanyintai and Lunshan formations have ΣREY ranges of 6.45—11.81 ppm (avg. 9.36 ppm) and 5.59—9.26 ppm (avg. 6.98 ppm), respectively. Both formations share remarkably similar REY distribution patterns (Fig. 5G, H), characterized by flat profiles with distinct positive Er anomalies. In contrast, the

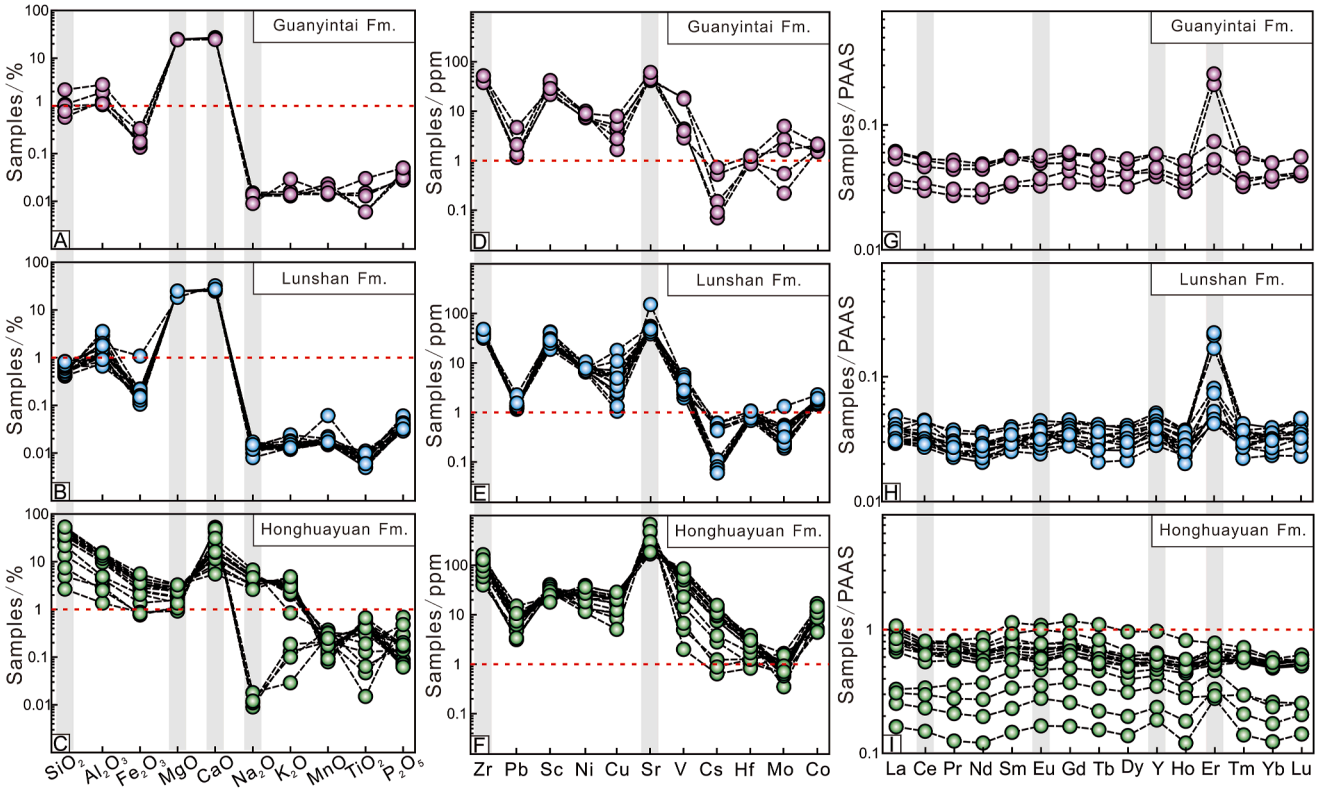

Fig. 5 Content changes of geochemistry from the Guanyintai, Lunshan, and Honghuayuan formations in the Sure 2 well. **A**—**C**) Major elements content; **D**—**F**) Trace elements content; **G**—**I**) Post-Archean Australian Shales (PAAS)-normalized REY patterns. Fm.: Formation.

Honghuayuan Formation has ΣREY ranging from 31.52 ppm to 171.22 ppm (avg. 123.64 ppm) and shows a slight leftward trend on the post-Archean Australian Shales (PAAS) standardization curve (Fig. 5l). In this study, Ce and Eu anomalies were calculated using the formulas $\delta Ce = 2Ce_N/(La_N + Pr_N)$ and $\delta Eu = 2Eu_N/(Sm_N + Gd_N)$ (Guo *et al.*, 2023), where the subscript N indicates PAAS standardization (McLennan, 1989). For the Guanyintai and Lunshan formations, δCe values range from 1.03 to 1.10 (avg. 1.06) and 1.01 to1.46 (avg. 1.19), respectively, while δEu values range from 0.58 to 0.63 (avg. 0.61) and 0.49 to 0.86 (avg. 0.64), respectively. Overall, δCe and δEu values in the Honghuayuan Formation range from 0.93 to 1.12 (avg. 1.01) and 0.54 to 0.73 (avg. 0.61), respectively.

5. Discussion

5.1. Sedimentary environment evolution

In the Ningzhen area, the Guanyintai Formation initiates with microbial mats dolostone (MF6), indicative of intertidal depositional conditions. Its upper succession transitions to brecciated dolostone (MF2), characterized by poorly sorted micritic clasts likely formed through karst collapse processes, suggesting supratidal exposure. The basal Lunshan Formation is dominated by various dolostone, including powder-crystal dolostone (MF1), lime-bearing powder-crystal dolostone (MF3), microbial mats dolostone (MF6) and laminated powder-crystal dolostone (MF7), representing a supratidal to upper tidal zone environment, with no significant sea level changes. In the middle succession, residual peloid dolostone (MF13) suddenly appeared, suggesting a significant sea-level change, then it returned to tidal flat environment, forming fine-grained dolostone (MF4). The Honghuayuan Formation is composed of calcic powder-crystal dolostone (MF3), peloidal packstone (MF10), and oolitic grainstone (MF11), documenting alternating supratidal and upper intertidal conditions.

In the Sure 1 well, the Lunshan Formation comprises predominantly powder-crystal dolostone (MF1) and fine crystal dolostone (MF4), suggesting sustained supratidal conditions, with rare residual oolitic dolostone (MF9) indicating ephemeral lagoonal incursions. The Honghuayuan Formation shows a shoal—lagoon systems environment, with occasional supratidal interbeds. Comparatively, the Sure 2 well Guanyintai Formation displays brecciated dolostone (MF2) within dominated sequences, suggesting enhanced supratidal exposure events. The Lunshan Formation maintains this supratidal environment, but suddenly appears residual peloid dolostone (MF13), suggesting a significant sea-level change in the mid-Lunshan Formation. The Honghuayuan interval transitions to dolomitized mudstone (MF8) interbedded with crinoid oolitic grainstone (MF12) and dolomitized bioclastic packstone (MF15), documenting mixed lower intertidal to subtidal shoal environments.

Microfacies analysis reveals that supratidal facies account for over 60% of Late Cambrian deposits, characterized by extensive peritidal—sabkha dolostones (e.g., Guanyintai Formation) reflecting the regional relative sea-level lowstand period. During this period, the alternation of supratidal brecciated dolostone (MF2) and intertidal microbial mats dolostone (MF6) (Ningzhen area) and powder-crystal dolostone (MF1) (Sure 2 well) indicates high-frequency sea-level fluctuations. These fluctuations likely resulted from combined effects of initial Caledonian uplift along the northern Yangtze margin and the Late Cambrian sea-level fall event (Haq and Schutter, 2008). This interpretation is further supported by strontium isotope and trace element characteristics (Ebneth *et al.*, 2001; Xu *et al.*, 2017). The Early Ordovician is characterized by the development of widespread tidal flat—Sabkha dolostone (Lunshan Formation) gradually transitioned to shallow-shoal bioclastic limestones (Honghuayuan Formation). The sea level has an overall upward trend, which is synchronized with the Early Ordovician transgression event (Haq and Schutter, 2008; Munnecke *et al.*, 2010). An abrupt occurrence of residual peloidal dolostone (MF13) within the upper Lunshan Formation records a brief regressive pulse correlative with equivalent strata in the Upper Yangtze region (Li *et al.*, 2016; Sun and Liu, 2017). The final closure of the South China paleo-ocean during the Late Paleozoic Caledonian Orogeny triggered rapid uplift of the Yangtze Block, terminating carbonate deposition in the Lower Yangtze region and initiating transition to siliciclastic basin fill (Zhang *et al.*, 2013; Xia *et al.*, 2018; Shu *et al.*, 2021). The persistent dolostone-dominated succession from the upper Guanyintai Formation to lower Lunshan Formation reflects stable sabkha-type depositional environments, whereas the appearance of oolitic-grainstone facies in upper Lunshan and Honghuayuan formations marks the establishment of high-energy shoal systems. This prolonged environmental stability provided optimal conditions for pervasive dolomitization throughout the study interval.

5.2. Behavior of elements during diagenesis

5.2.1. Non-carbonate contamination

REY cations are generally stable when incorporated into carbonate lattices. However, non-carbonate components such as terrigenous silicate minerals, sulfides, and iron-manganese oxides can be incorporated during deposition (Bayon *et al.*, 2004; Zhao *et al.*, 2009). Even minor contamination (e.g., 210 ppm) from terrigenous clasts can alter the REY patterns of marine carbonates, weakening La and Ce anomalies and reducing LREE depletion (Nothdurft *et al.*, 2004). The presence of such contaminants can be identified by correlations between ∑REY and elements like Al_2O_3 and Zr (indicative of terrigenous silicates), Pb and Sc (sulfides), and Ni and Cu (oxides) (Bolhar and Van Kranendonk, 2007; Jiang *et al.*, 2015). Samples from the Guanyintai and Lunshan formations show no evidence of such contamination, as supported by both elemental data and microfacies analysis (Fig. 6A, B, C, D). In contrast, the Honghuayuan Formation exhibits higher average contents of Al_2O_3, Zr, Pb, Ni, and SiO_2, suggesting significant contamination by terrigenous silicates, sulfides, and oxides. This contamination is confirmed by strong correlations between ∑REY and these elements (Fig. 6E, F, G, H), rendering the samples unsuitable for paleoenvironmental reconstruction.

5.2.2. Fluid source

The distributions of calcium and magnesium provide critical constraints on dolomitization processes (Zhang *et al.*, 2014). The MgO—CaO covariation diagram defines three distinct geochemical fields: limestone, dolostone, and contaminated (Fig. 7). Samples from the Lunshan and Guanyintai formations in the Sure 2 well and Nanjing area (Guo *et al.*, 2023) display a characteristic MgO—CaO negative correlation and cluster within the dolostone field, indicating a metasomatic origin with a consistent fluid source. In contrast, Honghuayuan Formation samples predominantly occupy the limestone contaminant zones, exhibiting marked rapid decrease in Ca with an increase in Mg, and showing high SiO_2 (avg. 31.64%) and Al_2O_3 (avg. 10.01%). These geochemical signatures, coupled with the characteristics of REY, confirm significant terrigenous input.

Iron and manganese provide critical burial diagenesis constraints. While seawater exhibits extremely low Fe—Mn concentrations, their concentrations in deep burial diagenetic pore fluids show a positive correlation with both burial depth and diagenetic alteration intensity (Allan and Wiggins, 1993). The dolostone of the Lunshan and Guanyintai formations exhibit low Fe_2O_3 (avg. 0.22% and 0.21%, respectively) and MnO concentrations (avg. 0.02% in both units). These values closely match the Fe_2O_3 (0.21%) and MnO

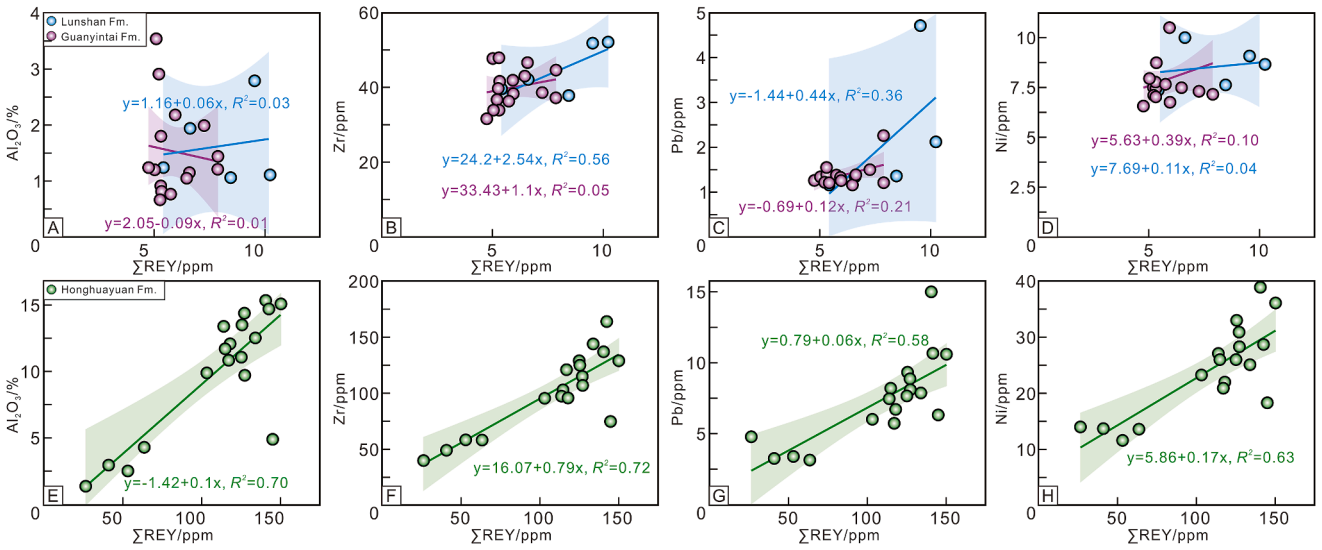

Fig. 6 The ∑REY and related elements covariation diagram of Guanyintai, Lunshan, and Honghuayuan formations from the Sure 2 well.

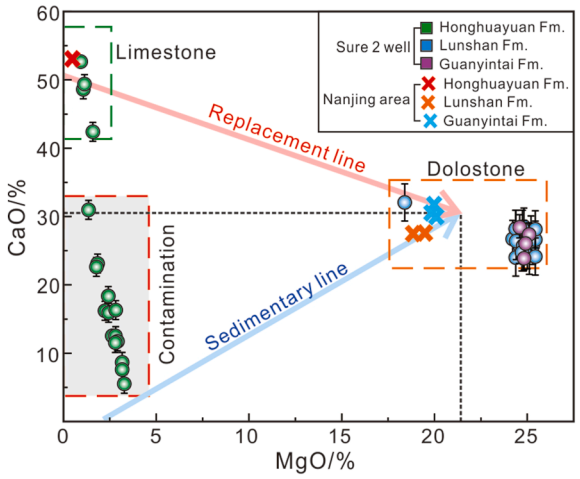

Fig. 7 The MgO—CaO covariation diagram of Guanyintai, Lunshan, and Honghuayuan formations from the Sure 2 well (Nanjing area data from Guo *et al.*, 2023).

(0.02%) contents observed in mudstone and grainstone in Nanjing area (Guo *et al.*, 2023). This geochemical coherence implies that the dolomitization fluids of the Lunshan and Guanyintai formations are similar to the fluid environment during limestone deposition, mainly influenced by seawater, and the dolomitization mainly occurs in near-surface environments.

In modern marine environments, calcium carbonate minerals, predominantly high-magnesium calcite and aragonite, precipitated directly from seawater, exhibit elevated Sr concentrations, ranging from 400 ppm to 5000 ppm in high-magnesium calcite and averaging 9800 ppm in aragonite (Kinsman, 1969). Given that the distribution coefficient of Sr in calcite is twice that in dolostone, Sr depletion commonly occurs during dolomitization and subsequent diagenesis. The timing of dolomitization critically influences Sr content, with early dolomitization yielding Sr-rich dolostone and late dolomitization producing Sr-poor dolostone. Additionally, diagenetic alteration by meteoric freshwater can further reduce Sr concentrations (Brand and Veizer, 1980; Veizer *et al.*, 1999). Compared to the high-magnesium calcite and aragonite, the Guanyintai and Lunshan formations exhibit significant Sr depletion, attributed to prolonged recrystallization during dolomitization and subsequent diagenesis under meteoric freshwater conditions. Microfacies analysis of the Guanyintai Formation reveals abundant brecciated dolostone (MF2), dissolved pore, and karst features, consistent with subaerial exposure and subsequent meteoric freshwater alteration during diagenesis.

The distribution patterns of REY in the dolostone of the Guanyintai and Lunshan formations are characterized by flat patterns and positive Y anomalies (Fig. 5G, H), closely resembling those of modern seawater (Bau *et al.*, 1996; Shields and Webb, 2004). This similarity implies that the REY compositions in these dolostone predominantly reflect the ambient seawater composition (Jiang *et al.*, 2015). Notably, these dolostone are distinguished by a significant positive Er anomaly (Fig. 5G, H), a feature not commonly observed in marine authigenic carbonates but consistent with the REY patterns found in deep-sea sediment pore waters of the Western Pacific (Deng *et al.*, 2017; Che *et al.*, 2021). Furthermore, the average δCe values of 1.06 and 1.19 for the Guanyintai and Lunshan formations, respectively, suggest diagenesis under mildly hypoxic conditions, indicative of pore water or a mixed pore water-seawater source in a burial environment.

5.3. *Genetic model of dolostone*

The three microfacies (MF1, MF2, MF6) of the Guanyintai Formation are mainly composed of powdery dolostone, and exhibit xenomorphic to subhedral textures with poor crystallinity and tight intergranular contacts, but preserving bird's eye and laminae structures (Fig. 8A, B). Combined with geochemical data, these characteristics suggest formation in a shallow burial environment. Systematic studies of Lower Yangtze carbonate diagenesis demonstrate no conclusive evidence for mixed-water dolomitization (Guo *et al.*, 2023). The mixed-water dolomitization model requires a more stable hydrological system than that of the Quaternary period, which is rarely observed in natural coastal zones, thus limiting its applicability and only has local significance (Hardie, 1987). The regional prevalence of powdery dolostone further precludes a mixed-water origin. Microfacies analysis shows that this period was in the relative sea-level lowstand, and intense evaporation generated Mg^{2+} enriched brines inside the platform which infiltrated downward and refluxed to dolomitization. During early diagenesis, the dolomitization degree was weak, and the carbonate sediments that had been initially consolidated and partially separated from the sedimentary water collapsed in situ, forming a large number of in-situ accumulated brecciated powder crystals. With the continuous progress of

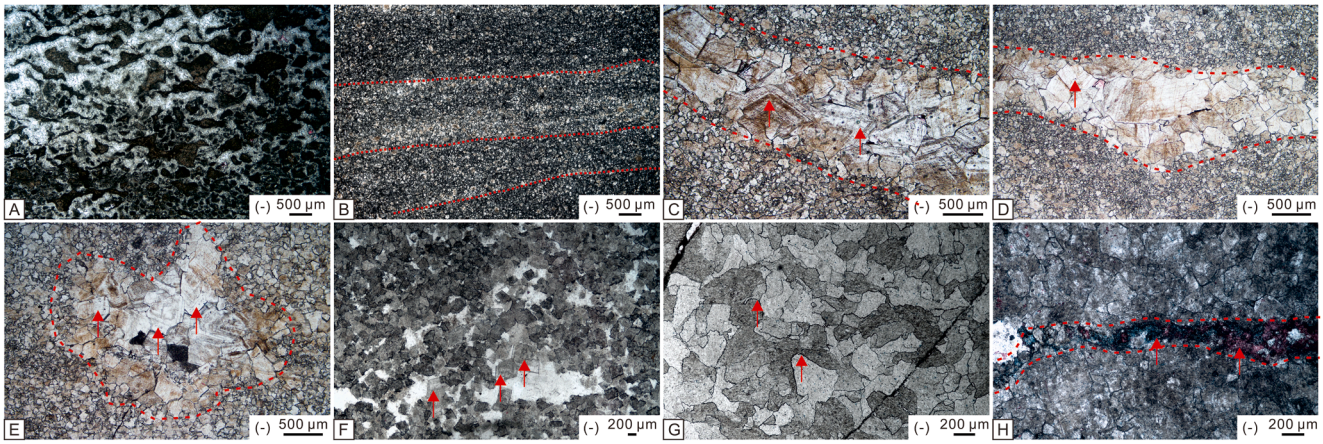

Fig. 8 Petrological evidence of hydrothermal dolomitization in the Lunshan sections, and the Sure 1 and 2 wells. **A**) Bird's eye in microbial mats dolostone; **B**) Laminae structures in powder-crystal dolostone; **C**—**E**) Grainy dolostone cement with ring characteristics (arrows); **F**) Saddle dolomite (arrows); **G**) Crystal-in-crystal features under hydrothermal activity (arrows); **H**) Ankerite cement (arrows). (-): plane-polarized light.

sedimentation, carbonate sediments entered a shallow burial period, the Mg^{2+} enrichment high salinity seawater continued to infiltrate and reflux downward through the pores between breccia. With the increase of burial depth, the Mg/Ca ratios of pore water increased, and the residual seawater continued to exchange with the original limestone, recrystallizing to form dolostone (Fig. 9A).

In contrast, the Lunshan Formation dolostone originated from hydrothermal alteration of marine limestone under burial conditions. Preservation of original grain morphology (MF9, MF13) indicates selective dolomitization in shallow burial settings. Ankerite and saddle dolomite are typical features indicating hydrothermal or other relatively high-temperature diagenetic environments (Machel and Lonnee, 2002; Davies and Smith, 2006). Under orthogonal polarized light, the crystal is saddle shaped, with wavy extinction, dirty surface and cleavage bending (Fig. 8C—G). Ankerite often filled in the pores as a cement, shown as purple under the microscope after staining (Fig. 8H). Hydrothermal action will also accelerate the dolomitization and recrystallized process, mostly heteromorphic and have obvious poikilitic characteristics (Fig. 8F, G). A pronounced positive δEu anomaly confirms hydrothermal alteration (Guo *et al.*, 2023). Early Paleozoic tectonic dynamics between the Yangtze and Cathaysia blocks generated widespread magmatic activity, particularly during Late Cambrian—Early Ordovician (Zhang *et al.*, 2013). Abundant diabase dikes in the Lunshan Formation further confirmed the magmatic activity, and geothermal anomalies from magmatism facilitated upward fluid migration, driving Mg^{2+} enrichment fluid circulation (seawater or hydrothermal) during burial dolomitization (Fig. 9B).

Integrated carbonate microfacies analysis and geochemical data reveal that the Early Paleozoic dolostone in the Lower Yangtze region exhibit distinct dual-phase genetic characteristics, marked by the synergistic effects of early-stage evaporative reflux (Guanyintai Formation) and late-stage burial—hydrothermal overprinting (Lunshan Formation). In contrast to the single-phase reflux-dominated mechanisms documented in the Upper Yangtze region (e.g., Longwangmiao Formation, Sichuan Basin) (Ren *et al.*, 2016; Liu *et al.*, 2021), the complex diagenetic history of the Lower Yangtze dolostone highlights the critical control of tectonic activities along the cratonic margin (e.g., Caledonian faulting—magmatism) on fluid sources. The hydrothermal characteristics of the Lunshan Formation (such as saddle dolomite textures and positive δEu anomaly) bear similarities to those of the Tarim Basin (Liu *et al.*, 2022). However, the elevated terrigenous input in the Honghuayuan Formation (avg. 10.01%) reflects a unique paleogeographic setting driven by proximal clastic supply from the uplifted Cathaysian Block. These findings underscore that while Early Paleozoic dolomitization processes were broadly modulated by global eustasy (Choquette and Hiatt, 2008; Jiang *et al.*, 2023), regional tectono-sedimentary frameworks ultimately

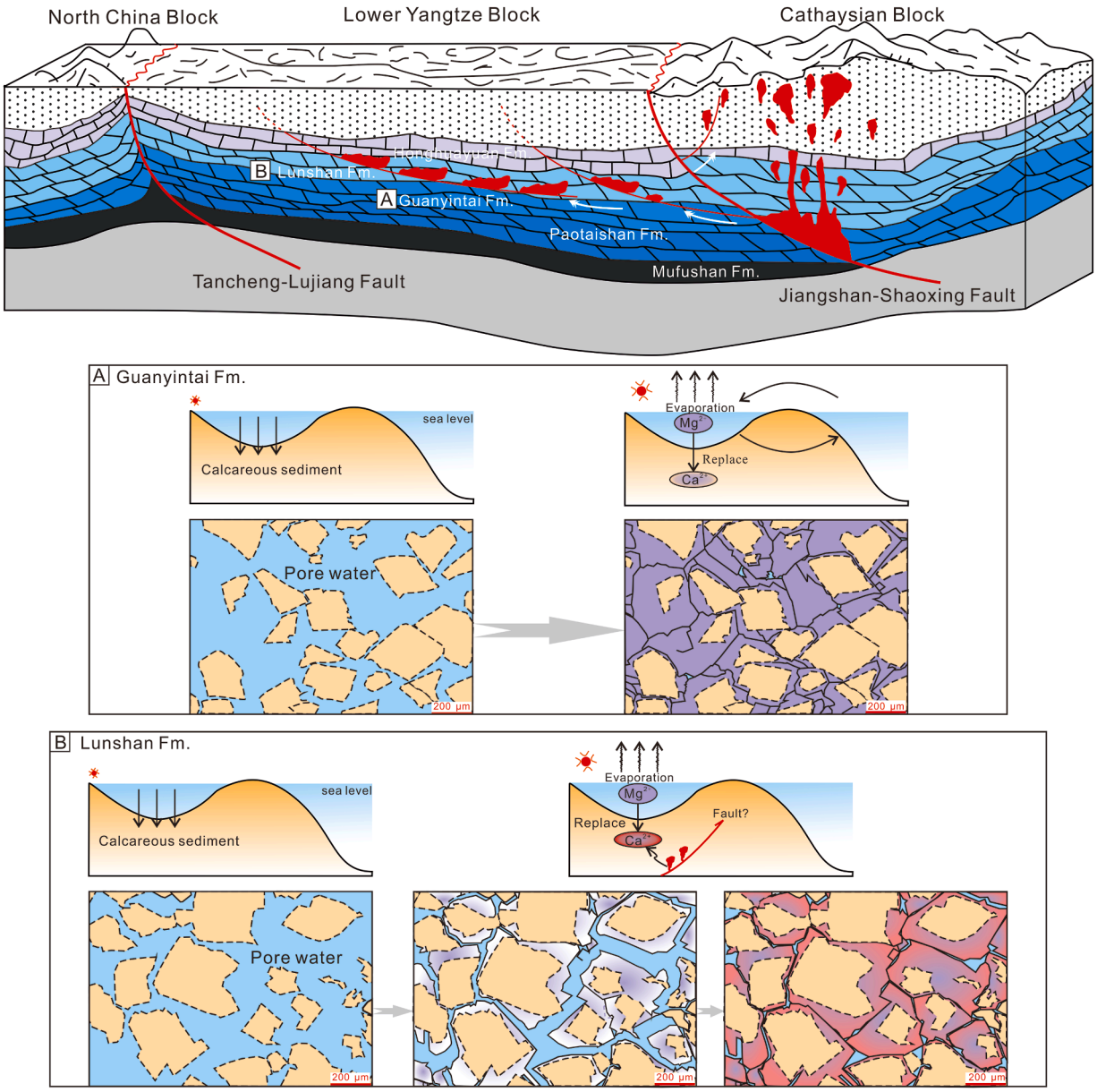

Fig. 9 Genetic model of dolostone in the Guanyintai and Lunshan formations of the Sure 2 well. **A**) The downward infiltration and reflux of high-salinity seawater rich in Mg^{2+} into early calcareous sediments, leading to an increase in the Mg/Ca ratio of pore water and dolomitization; **B**) The selective dolomitization due to early reflux infiltration, followed by the influx of Mg^{2+} enrichment fluids from hydrothermal activity, which accelerates the dolomitization process and forms significant saddle dolomite.

governed the spatiotemporal heterogeneity of diagenesis through their regulation of fluid chemistry and migration efficiency.

6. Conclusions

The Early Paleozoic carbonates in the Lower Yangtze region consist of 15 microfacies types, with the Guanyintai and Lunshan formations dominated by fine-grained dolostone from tidal flats, and the Honghuayuan Formation featuring grainstone from a shallow bank.

Geochemical analysis of the Guanyintai and Lunshan formations fluid source suggests pore water or a mixture of seawater and pore water, while the Honghuayuan Formation shows contamination by terrigenous materials.

The comprehensive study shows that the dolostone in the Guanyintai Formation of the Lower Yangtze region was formed through a percolation reflux dolomitization model under a shallow burial environment,

while the dolostone in the Lunshan Formation resulted from the superimposition of burial dolomitization and hydrothermal dolomitization.

CRediT authorship contribution statement

Jia-Wei He conceived the study, designed the methodology, and drafted the manuscript. **Tao Deng** performed the experiments and data collection. **Li-Juan Wang** carried out the formal analysis and created the visualizations. **Jun-Peng Guan** participated in data interpretation and reviewed the manuscript. **Yong-Biao Yang** acquired funding and provided resources. **Xiu-Mian Hu** supervised the project and critically revised the manuscript. All authors read and approved the final manuscript.

Declaration of competing interest

The authors declare that they have no known competing financial interests or personal relationships that could have appeared to influence the work reported in this paper.

Acknowledgements

We would like to express our sincere gratitude to the Carbon Peak and Carbon Neutralization Science and Technology Innovation Special Fund of Jiangsu Province, China (Grants No. BE2022859, BE2022034-1).

References

Allan, J.R., Wiggins, W.D., 1993. *Dolomite Reservoirs: Geochemical Techniques for Evaluating Origin and Distribution. AAPG Continuing Education Course Notes Series*, 36. American Association of Petroleum Geologists, Tulsa, Oklahoma, U.S.A. https://doi.org/10.1306/CE36576.

Bai, Z.Z., Shi, S.Y., Hu, Y.J., Yang, W., Xie, W.R., Li, W.Z., 2025. Dolomitization history and porosity evolution of the deeply buried Cambrian Xixiangchi Formation, Sichuan Basin, SW China. *Journal of Palaeogeography*, 14(3), 100258. https://doi.org/10.1016/j.jop.2025.100258.

Bau, M., Koschinsky, A., Dulski, P., Hein, J.R., 1996. Comparison of the partitioning behaviours of yttrium, rare earth elements, and titanium between hydrogenetic marine ferromanganese crusts and seawater. *Geochimica et Cosmochimica Acta*, 60(10), 1709—1725. https://doi.org/10.1016/0016-7037(96)00063-4.

Bayon, G., German, C.R., Burton, K.W., Nesbitt, R.W., Rogers, N., 2004. Sedimentary Fe—Mn oxyhydroxides as paleoceanographic archives and the role of aeolian flux in regulating oceanic dissolved REE. *Earth and Planetary Science Letters*, 224(3—4), 477—492. https://doi.org/10.1016/j.epsl.2004.05.033.

Bolhar, R., Van Kranendonk, M.J., 2007. A non-marine depositional setting for the northern Fortescue Group, Pilbara Craton, inferred from trace element geochemistry of stromatolitic carbonates. *Precambrian Research*, 155(3—4), 229—250. https://doi.org/10.1016/j.precamres.2007.02.002.

Brand, U., Veizer, J., 1980. Chemical diagenesis of a multicomponent carbonate system—1: Trace elements. *Journal of Sedimentary Petrology*, 50(4), 1219—1236. https://doi.org/10.1306/212F7BB7-2B24-11D7-8648000102C1865D.

Cai, Z.R., Xia, B., Huang, Q.T., Wan, Z.F., 2015. Comparative study of the tectonic setting on the formation and preservation of Paleozoic shale gas between the Upper Yangtze and the Lower Yangtze Platforms. *Natural Gas Geoscience*, 26(8), 1446—1454. https://doi.org/10.11764/j.issn.1672-1926.2015.08.1446 (in Chinese with English abstract).

Cai, W.K., Liu, J.H., Zhou, C.H., Keeling, J., Glasmacher, U.A., 2021. Structure, genesis and resources efficiency of dolomite: New insights and remaining enigmas. *Chemical Geology*, 573, 120191. https://doi.org/10.1016/j.chemgeo.2021.120191.

Chai, F.Y., 2019. Study on Paleozoic sedimentary facies and favorable area evaluation in lower Yangtze basin. *Reservoir Evaluation and Development*, 9(2), 7—12. https://doi.org/10.3969/j.issn.2095-1426.2019.02.002 (in Chinese with English abstract).

Che, H., Hu, B.Q., Ding, X., Song, W.Y., Guo, J.W., Cui, R.Y., Deng, Y.N., 2021. Rare earth element geochemistry characteristics and implications of pore-water from deep sea sediment in Western Pacific Ocean. *Marine Geology and Quaternary Geology*, 41(1), 75—86. https://doi.org/10.16562/j.cnki.0256-1492.2020102601 (in Chinese with English abstract).

Chen, Z., Wang, L.J., Li, J., He, J.W., Yang, Y.B., Deng, T., Guan, J.P., Gong, H.T., Hu, X.M., 2024. Early Paleozoic carbonate microfacies and sedimentary environment evolution in the lower Yangtze area. *Acta Sedimentologica Sinica*, 42(6), 2191—2203. https://doi.org/10.14027/j.issn.1000-0550.2023.026 (in Chinese with English abstract).

Choquette, P.W., Hiatt, E.E., 2008. Shallow-burial dolomite cement: A major component of many ancient sucrosic dolomites. *Sedimentology*, 55(2), 423—460. https://doi.org/10.1111/j.1365-3091.2007.00908.x.

Davies, G.R., Smith, L.B.J., 2006. Structurally controlled hydrothermal dolomite reservoir facies: An overview. *AAPG Bulletin*, 90(11), 1641—1690.

Deng, Y.N., Ren, J.B., Guo, Q.J., Cao, J., Wang, H.F., Liu, C.H., 2017. Rare earth element geochemistry characteristics of seawater and porewater from deep sea in western Pacific. *Scientific Reports*, 7, 16539. https://doi.org/10.1038/s41598-017-16379-1.

Dunham, R.J., 1962. Classification of carbonate rocks according to depositional texture. In: Ham, W.E. (Ed.), *Classification of Carbonate Rocks — A Symposium*, vol. 1. AAPG Memoir, pp. 108—121.

Ebneth, S., Shields, G.A., Veizer, J., Miller, J.F., Shergold, J.H., 2001. High-resolution strontium isotope stratigraphy across the Cambrian—Ordovician transition. *Geochimica et Cosmochimica Acta*, 65(14), 2273—2292. https://doi.org/10.1016/S0016-7037(01)00580-4.

Embry, A.F., Klovan, J.E., 1971. A Late Devonian reef tract on northeastern Banks Islands, N.W.T. *Bulletin of Canadian Petroleum Geology*, 19(4), 730—781. https://doi.org/10.35767/gscpgbull.19.4.730.

Fan, D.J., Luan, G.Z., Li, S.T., Guo, Z.G., 1996. The origin of dolostones appear in Upper Sinian and Paleozoic, Tangshan, Nanjing. *Transaction of Oceanology and Limnology*, 18(3), 26—32 (in Chinese with English abstract).

Fang, C.G., Huang, Z.Q., Teng, L., Xu, F.F., Zhou, D.R., Yin, Q.C., Shao, W., Shi, G., 2020. Lithofacies palaeogeography of the Late Ordovician Kaitian Stage—the early Silurian Rhuddanian Stage in Lower Yangtze region and its petroleum geological significance. *Geology in China*, 47(1), 144—160. https://doi.org/10.12029/gc20200112 (in Chinese with English abstract).

Flügel, E., 2010. *Microfacies of Carbonate Rocks: Analysis, Interpretation and Application*. Springer, Berlin, Heidelberg. https://doi.org/10.1007/978-3-642-03796-2.

Folk, R.L., 1962. Spectral subdivision of limestone types. In: Ham, W.E. (Ed.), *Classification of Carbonate Rocks — A Symposium*, vol. 1. AAPG Memoir, pp. 62—84.

Gao, X., Fang, C.G., Huang, Z.Q., Meng, L.N., Ye, J., Li, J.Q., Li, F.J., 2023. Lithofacies paleogeography and shale oil and gas prospective analysis of the Ordovician Ningguo-Hule period in the Lower Yangtze region. *Geology in China*, 50(4), 1122—1137. https://doi.org/10.12029/gc20190703001 (in Chinese with English abstract).

Gregg, J.M., Bish, D.L., Kaczmarek, S.E., Machel, H.G., 2015. Mineralogy, nucleation and growth of dolomite in the laboratory and sedimentary environment: A review. *Sedimentology*, 62(6), 1749—1769. https://doi.org/10.1111/sed.12202.

Guo, Y., Du, X.F., Yang, B., Huang, Z., Wang, J., Li, Z.Q., 2023. Geochemical characteristics and genesis of Upper Sinian—Lower Paleozoic dolomite in Lower Yangtze region: A case study from Nanjing area. *Earth Science*, 48(12), 4558—4574. https://doi.org/10.3799/dqkx.2022.492 (in Chinese with English abstract).

Haq, B.U., Schutter, S.R., 2008. A chronology of Paleozoic sea-level changes. *Science*, 322(5898), 64—68. https://doi.org/10.1126/science.1161648.

Hardie, L.A., 1987. Dolomitization: A critical view of some current views. *Journal of Sedimentary Petrology*, 57(1), 166—183.

He, Z.L., Ma, Y.S., Zhang, J.T., Zhu, D.Y., Qian, Y.X., Ding, Q., Chen, D.Z., 2020. Distribution, genetic mechanism and control factors of dolomite and dolomite reservoirs in China. *Oil & Gas Geology*, 41(1), 1—14. https://doi.org/10.11743/ogg20200101 (in Chinese with English abstract).

Jiang, L., Cai, C.F., Worden, R.H., Li, K.K., Xiang, L., Chu, X.L., Shen, A.J., Li, W.J., 2015. Rare earth element and yttrium (REY) geochemistry in carbonate reservoirs during deep burial diagenesis: Implications for REY mobility during thermochemical sulfate reduction. *Chemical Geology*, 415, 87—101. https://doi.org/10.1016/j.chemgeo.2015.09.010.

Jiang, H.C., Liang, J.T., Azmy, K., Cao, J.X., Wen, L., Zhou, G., He, Y., Liu, S.B., Huo, F., Wen, H.G., 2023. Controls of sedimentary facies and sealevel fluctuation on dolomitization: The Lower Cambrian Longwangmiao Formation in Sichuan Basin, China. *Marine and Petroleum Geology*, 157, 106465. https://doi.org/10.1016/j.marpetgeo.2023.106465.

Kinsman, D.J.J., 1969. Interpretation of Sr^{2+} concentrations in carbonate minerals and rocks. *Journal of Sedimentary Petrology*, 39(2), 486—508. https://doi.org/10.1306/74D71CB7-2B21-11D7-8648000102C1865D.

Li, J.H., Zhang, Y.Q., Dong, S.W., Johnston, S.T., 2014. Cretaceous tectonic evolution of South China: A preliminary synthesis. *Earth-Science Reviews*, 134, 98—136. https://doi.org/10.1016/j.earscirev.2014.03.008.

Li, J.T., Liu, J.B., Sun, Y.C., Yan, Z., Wu, R.C., Zhan, R.B., 2016. On the Lower Ordovician Lunshan Formation in Lower Yangtze region, South China: Its petrology, stratigraphy and palaeogeography. *Journal of Palaeogeography (Chinese Edition)*, 18(3), 411—423. https://doi.org/10.7605/gdlxb.2016.03.029 (in Chinese with English abstract).

Li, F.J., Ma, X.K., Lai, X.L., 2022. Petrography, geochemistry and genesis of dolomites in the upper Cambrian Sanshanzi Formation of the western Ordos Basin, northern China. *Journal of Asian Earth Sciences*, 223, 104980. https://doi.org/10.1016/j.jseaes.2021.104980.

Liu, D.W., Cai, C.F., Hu, Y.J., Peng, Y.Y., Jiang, L., 2021. Multistage dolomitization and formation of ultra-deep Lower Cambrian Longwangmiao Formation reservoir in central Sichuan Basin, China. *Marine and Petroleum Geology*, 123, 104752. https://doi.org/10.1016/j.marpetgeo.2020.104752.

Liu, Y.N., Ngia, N.R., Hu, M.Y., Cai, Q.S., 2022. Evaluation of the properties of dolomitization fluids and diagenetic alterations of Mg/Ca ratios in carbonate rocks in the Cambrian Series-2 to Miaolingian strata in Central Uplift Belt, Tarim Basin: Constraints from halogens, REEs and isotope geochemistry. *Marine and Petroleum Geology*, 144, 105838. https://doi.org/10.1016/j.marpetgeo.2022.105838.

Liu, P., Chen, Z.S., Wang, G.L., Mao, T., Li, C., Zhou, Y.N., Xie, H., Xiang, T., 2024. Hydrogeochemical signatures origin of a karst geothermal reservoir—the Sinian Dengying Formation in northern Guizhou, China. *Geosciences Journal*, 28(1), 107—123. https://doi.org/10.1007/s12303-023-0030-9.

Machel, H.G., Lonnee, J., 2002. Hydrothermal dolomite—A product of poor definition and imagination. *Sedimentary Geology*, 152(3—4), 163—171. https://doi.org/10.1016/S0037-0738(02)00259-2.

McLennan, S.M., 1989. Rare earth elements in sedimentary rocks: Influence of provenance and sedimentary processes. *Reviews in Mineralogy and Geochemistry*, 21(1), 169—200.

Metcalfe, I., 2011. Tectonic framework and Phanerozoic evolution of Sundaland. *Gondwana Research*, 19(1), 3—21. https://doi.org/10.1016/j.gr.2010.02.016.

Munnecke, A., Calner, M., Harper, D.A.T., Servais, T., 2010. Ordovician and Silurian sea-water chemistry, sea level, and climate: A synopsis. *Palaeogeography, Palaeoclimatology, Palaeoecology*, 296(3—4), 389—413. https://doi.org/10.1016/j.palaeo.2010.08.001.

Noffke, N., Awramik, S.M., 2013. Stromatolites and MISS: Differences between relatives. *GSA Today*, 23(9), 4—9. https://doi.org/10.1130/GSATG187A.1.

Nothdurft, L.D., Webb, G.E., Kamber, B.S., 2004. Rare earth element geochemistry of Late Devonian reefal carbonates, Canning Basin, Western Australia: Confirmation of a seawater REE proxy in ancient limestones. *Geochimica et Cosmochimica Acta*, 68(2), 263—283. https://doi.org/10.1016/S0016-7037(03)00422-8.

Petrash, D.A., Bialik, O.M., Bontognali, T.R.R., Vasconcelos, C., Roberts, J.A., McKenzie, J.A., Konhauser, K.O., 2017. Microbially catalyzed dolomite formation: From near-surface to burial. *Earth-Science Reviews*, 171, 558—582. https://doi.org/10.1016/j.earscirev.2017.06.015.

Qu, H.Z., Yan, Z.X., Zheng, C., Xu, W., He, F.W., Sun, Q.M., Zhang, X.Y., Li, M.X., 2023. Quantitative characterization and origin of differences in pore parameter distribution: A case study of the lower Cambrian Longwangmiao Formation in the Gaoshiti area of central Sichuan Basin. *Frontiers in Earth Science*, 10, 1043148. https://doi.org/10.3389/feart.2022.1043148.

Randazzo, A.F., Zachos, L.G., 1984. Classification and description of dolomitic fabrics of rocks from the Floridan aquifer, U.S.A. *Sedimentary Geology*, 37(3), 151—162. https://doi.org/10.1016/0037-0738(84)90005-8.

Ren, Y., Zhong, D.K., Gao, C.L., Yang, X.Q., Xie, R., Li, Z.P., Deng, M.X., Zhou, Y.C., 2016. Geochemical characteristics, genesis and hydrocarbon significance of dolomite in the Cambrian Longwangmiao Formation, eastern Sichuan Basin. *Acta Petrolei Sinica*, 37(9), 1102—1115. https://doi.org/10.7623/syxb201609004 (in Chinese with English abstract).

Riding, R., 2000. Microbial carbonates: The geological record of calcified bacterial—algal mats and biofilms. *Sedimentology*, 47(s1), 179—214. https://doi.org/10.1046/j.1365-3091.2000.00003.x.

Shan, H.S., Liu, J.L., Ding, X., Chen, X.Y., Yu, X.Q., Liu, Z.H., Xu, Z.Y., 2022. Subduction initiation of the Proto-Tethys Ocean that facilitated climate change and biodiversification. *Earth and Planetary Science Letters*, 600, 117874. https://doi.org/10.1016/j.epsl.2022.117874.

Shang, W.L., Xu, S.H., Li, X.G., Liang, F., Wu, C., Wang, J.S., Li, Z.J., Sun, Y.H., Li, Y.H., Li, M., Xu, Z.J., Tian, Z., 2023. Utilizing 2D seismic forward modeling to constrain the seismic response and plane distribution of grain shoal reservoir in the northern slope of Central Sichuan Paleo-uplift, Sichuan Basin. *Marine and Petroleum Geology*, 152, 106228. https://doi.org/10.1016/j.marpetgeo.2023.106228.

Shields, G.A., Webb, G.E., 2004. Has the REE composition of seawater changed over geological time? *Chemical Geology*, 204(1—2), 103—107. https://doi.org/10.1016/j.chemgeo.2003.09.010.

Shu, L.S., Yao, J.L., Wang, B., Faure, M., Charvet, J., Chen, Y., 2021. Neoproterozoic plate tectonic process and Phanerozoic geodynamic evolution of the South China Block. *Earth-Science Reviews*, 216, 103596. https://doi.org/10.1016/j.earscirev.2021.103596.

Sun, Y.C., Liu, J.B., 2017. Sea-level fluctuations in the Tremadocian of the Ordovician in the Upper Yangtze region of South China. *Acta Scientiarum Naturalium Universitatis Pekinensis*, 53(1), 66—80. https://doi.org/10.13209/j.0479-8023.2016.123 (in Chinese with English abstract).

Van Lith, Y., Warthmann, R., Vasconcelos, C., McKenzie, J.A., 2003. Sulphate-reducing bacteria induce low-temperature Ca-dolomite and high Mg-calcite formation. *Geobiology*, 1(1), 71—79. https://doi.org/10.1046/j.1472-4669.2003.00003.x.

Veizer, J., Ala, D., Azmy, K., Bruckschen, P., Buhl, D., Bruhn, F., Carden, G.A.F., Diener, A., Ebneth, S., Godderis, Y., Jasper, T., Korte, C., Pawellek, F., Podlaha, O.G., Strauss, H., 1999. $^{87}Sr/^{86}Sr$, $\delta^{13}C$ and $\delta^{18}O$ evolution of Phanerozoic seawater. *Chemical Geology*, 161(1—3), 59—88. https://doi.org/10.1016/S0009-2541(99)00081-9.

Wang, Y.J., Fan, W.M., Zhang, G.W., Zhang, Y.H., 2013. Phanerozoic tectonics of the South China Block: Key observations and controversies. *Gondwana Research*, 23(4), 1273—1305. https://doi.org/10.1016/j.gr.2012.02.019.

Wilson, J.L., 1975. *Carbonate Facies in Geologic History*. Springer-Verlag, Berlin.

Wu, R.C., Liu, J.B., Calner, M., Gong, F.Y., Lehnert, O., Luan, X.C., Li, L.X., Zhan, R.B., 2020. High-resolution carbon isotope stratigraphy of the Lower and Middle Ordovician succession of the Yangtze Platform, China: Implications for global correlation. *Journal of the Geological Society*, 177(3), 537—549. https://doi.org/10.1144/jgs2018-208.

Xia, Z.L., Hua, C.X., Liu, J.Y., Yu, H., 2018. Favorable Lower Paleozoic exploration targets in the Lower Yangtze region. *Marine Geology and Quaternary Geology*, 38(3), 66—74 (in Chinese with English abstract).

Xu, Z.J., Lan, Y.Z., Cheng, R.H., Li, S.L., 2017. Carbonate geochemical record of sea-level change of Lunshan Formation in Lower Ordovician in Jurong area. *Journal of Jilin University (Earth Science Edition)*, 47(5), 1458—1470. https://doi.org/10.13278/j.cnki.jjuese.201705110 (in Chinese with English abstract).

Yang, S., Yang, H.Z., Peng, X., Lan, X.M., Yang, Y.F., Zhao, Y., Zhang, K., Chen, H.D., 2023. Research of

influencing factors on permeability for carbonate rocks based on LBM simulation: A case study of low-permeability gas reservoir of Sinian Dengying Formation in Sichuan Basin. *Frontiers in Earth Science*, 11, 1091431. https://doi.org/10.3389/feart.2023.1091431.

Zhang, H., Zhou, L.Q., Li, J.Q., 2006. Hydrocarbon exploration potential analysis of the lower marine formation assemblage in the Lower Yangtze region. *Petroleum Geology and Experiment*, 28(1), 15—20. https://doi.org/10.3969/j.issn.1001-6112.2006.01.003 (in Chinese with English abstract).

Zhang, G.W., Guo, A.L., Wang, Y.J., Li, S.Z., Dong, Y.P., Liu, S.F., He, D.F., Cheng, S.Y., Lu, R.K., Yao, A.P., 2013. Tectonics of South China continent and its implications. *Science China Earth Sciences*, 56(11), 1804—1828. https://doi.org/10.1007/s11430-013-4679-1.

Zhang, W., Guan, P., Jian, X., Feng, F., Zou, C.N., 2014. In situ geochemistry of Lower Paleozoic dolomites in the northwestern Tarim Basin: Implications for the nature, origin, and evolution of diagenetic fluids. *Geochemistry, Geophysics, Geosystems*, 15(7), 2744—2764. https://doi.org/10.1002/2013GC005194.

Zhang, K., Liu, Z.P., Xu, Z.T., Chang, Q., Fathy, D., Liu, R., Bai, E., 2024. Microbial and hydrothermal dolomite formation in Early Cretaceous lacustrine sediments in Yin'e Basin: Insights from petrology and geochemistry. *Sedimentary Geology*, 471, 106739. https://doi.org/10.1016/j.sedgeo.2024.106739.

Zhao, Y.Y., Zheng, Y.F., Chen, F.K., 2009. Trace element and strontium isotope constraints on sedimentary environment of Ediacaran carbonates in southern Anhui, South China. *Chemical Geology*, 265(3—4), 345—362. https://doi.org/10.1016/j.chemgeo.2009.04.015.

Zhou, J.G., Xu, Z.H., Huan, S.W., Li, W.Z., Duan, J.M., Zhu, Y.J., Zheng, J.F., Wu, D.X., Chang, S.Y., 2024. Frontiers and trends in the research on carbonate sedimentology and reservoir geology. *Oil & Gas Geology*, 45(4), 929—953. https://doi.org/10.11743/ogg20240404 (in Chinese with English abstract).

Supplementary data

Supplementary data to this article can be found online at https://doi.org/10.1016/j.jop.2026.100338.

Supplementary data include geochemical analysis process and Tables S1 and S2.

Table S1 Major and Trace Elements test results.

Table S2 Rare Earth elements and Yttrium test results.